GRID SIDE CONVERTER BASED SHUNT ACTIVE POWER FILTER OF VARIABLE SPEED DOUBLY FED INDUCTION GENERATOR DRIVEN BY WIND TURBINE

Gaber EL-Saady Ahmed[1], EL-Noby Ahmed Ibrahim[2], Hazem Hassan Ali[3]

[1,2,3] Electrical Engineering Department, Assiut University, Assiut, Egypt, hazemhassan481@yahoo.com

Abstract - This paper presents power quality improvement by using Grid Side Converter (GSC) of variable speed Wind Energy Conversion System (WECS) based Shunt Active Power Filter (SAPF). Maximum Power Point Tracking (MPPT) is carried out by its Rotor Side Converter (RSC) using Genetic Algorithm (GA). The optimal Tip Speed Ratio (TSR) is determined to extract the maximum available wind power at any wind speed until rated wind speed. Doubly Fed Induction Generator (DFIG) has stator terminals are connected directly to the grid. However, the rotor terminals of DFIG are connected to the mains via a partially rated variable frequency ac/dc/ac converter. The ac/dc/ac converter system is consisting of RSC and GSC are connected back-to-back by a DC-link capacitor. Stator Voltage Orientation (SVO) is the principle control for both RSC and GSC controlled by hysteresis current controller. The GSC has two functions the first function is to keep the DC link voltage constant at its level and get unity power factor for GSC of DFIG. The second function is acting as SAPF to obtain unity power factor at power grid side due to presence of inductive load and cancel current harmonic due to presence of nonlinear load at Point of Common Coupling (PCC) connected in parallel with inductive load. The system under study is simulated using MATLAB/Simulink package. The digital simulation results show that the output power and rotor speed response for step change in wind speed prove the effectiveness and powerful of the proposed GA controller for MPPT and also achievement of the power quality improvement.

Keywords – *DFIG, MPPT, Genetic Algorithm, Shunt Active Power Filter, Wind Turbine Control.*

1. Introduction

Electricity generation from renewable resources, and particularly from the wind, is considered today as a competitive and necessary alternative to fossil resources. Wind turbines can operate with either fixed speed or variable speed. Pitch-adjusting variable-speed wind turbines like DFIG have become the dominating type of yearly installed wind turbines in recent years. Several reasons for choosing DFIG, such as the reduction of both the mechanical structure stresses and the possibility to control four quadrant active and reactive power capabilities, have been chosen for variable speed operation of wind turbines. The variable speed wind turbine can provide decoupled control of active and reactive power of the generator and improve power quality [1]. Due to several integration of nonlinear loads, such as power electronics and large AC drives, which are polluting sources of the power grid, the modern WECS is not only controlled to product active power to the customers but also to improve the power quality under different conditions. The power electronic converters has the ability to achieve reactive power compensation to achieve voltage control and to eliminate harmonic currents. Recently, WECS converters of DFIG connected between the rotor terminals of generator and the grid has been developed to have capability to improve grid power quality and achieve harmonic currents mitigation [2,3]. In this work, GSC is used as SAPF to compensate the phase shift due to presence of inductive load and to eliminate current harmonic and get unity power factor due to presence of nonlinear load at PCC connected in shunt with inductive load in addition to its main function which is keeping the voltage of the DC link constant at its level and achieving unity power factor of GSC of DFIG. For MPPT, the speed controller can continuously adjust the speed of the rotor to maintain TSR constant at the level which gives the maximum power coefficient and then the efficiency of the turbine will be significantly increased, the generator is controlled by power electronic equipment, which makes it possible to control the rotor speed in low wind speed below rated value [4]. In this way the power fluctuations caused by wind variations can be more or less absorbed by changing the rotor speed and thus power variations originating from the wind conversion and the drive train can be reduced. Therefore, control systems for DFIG variable speed wind turbines should continue to evolve towards more and more effective and innovative solutions. Wind energy, even though abundant, varies continually as wind speed changes throughout the day. Amount of power output from a WECS depends upon the accuracy with which the peak power points are tracked by the MPPT controller of the WECS control system irrespective of the type of generator used. The maximum power extraction algorithms researched so far can be classified into three

main control methods, were presented and studied in [5]. The TSR control is one of the main control methods which regulates the rotational speed of the generator in order to maintain the TSR to an optimum value at which power extracted is maximum. This method requires both the wind speed and the turbine speed to be measured or estimated.

2. Operating region and aerodynamics of the wind turbine

A. Operating region of the wind turbine

The wind turbine operates, with different dynamics, from the cut-in wind speed (usually 4 m/s, for modern wind turbines) to the cut-out wind speed (around 24 m/s), as shown in Fig. 1. Three distinct wind speed points can be noticed in this power curve [6]:

1) $V_{\text{wind\_Cut-in}}$: The lowest wind speed at which wind turbine starts to generate power.
2) Rated wind speed: Wind speed at which the wind turbine generates the rated power, which is usually the maximum power wind turbine can produce.
3) $V_{\text{wind\_Cut-out}}$ :: Wind speed at which the turbine ceases power generation and is shut down (with automatic brakes and/or blade pitching) to protect the turbine from mechanical damage.
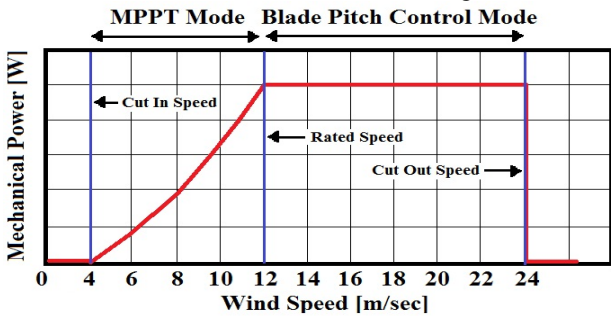

Fig. 1 Power curve of a variable speed wind turbine.

B. Aerodynamic of the wind turbine

The energy conversion in a wind turbine can be described by the nonlinear equations [7], [8]:

$$P_m = 0.5\rho A V_w^{\,3} C_p \qquad (1)$$

Where P_m is the mechanical power (Watt), ρ is the air density (kg/m^3), $A = \pi R^2$ is area covered by turbine blades (m^2), R is rotor radius (m), V_w is the velocity of available wind (m/sec) and C_p is the coefficient of power. The power captured by the wind turbine depends highly on C_p for a given wind speed. The relationship of C_p with λ and β represents output characteristics of the wind turbine as in (2):

$$C_p(\lambda, \beta) = 0.5176\left(\frac{116}{\lambda_i} - 0.4\beta - 5\right) e^{-\frac{21}{\lambda_i}} + 0.0068\lambda \quad (2)$$

Where λ is TSR , a variable expressing the linear speeds of blade tip to speed of wind and β is the pitch

angle, λ and $\frac{1}{\lambda_i}$ can be expressed as in (3) and (4), respectively.

$$\lambda = \frac{w_t R}{V_w} \qquad (3)$$

Where w_t is rotational turbine speed (rad/sec).

$$\frac{1}{\lambda_i} = \frac{1}{\lambda + 0.08\beta} - \frac{0.035}{\beta^3 + 1} \qquad (4)$$

By using (2), the typical C_p versus λ curve at different pitch angle β is shown in Fig. 2. As aforementioned, there is an optimum value of λ that leads to maximum power coefficient $C_{p,max}$. The maximum theoretical value of Cp is approximately 0.59 [9].
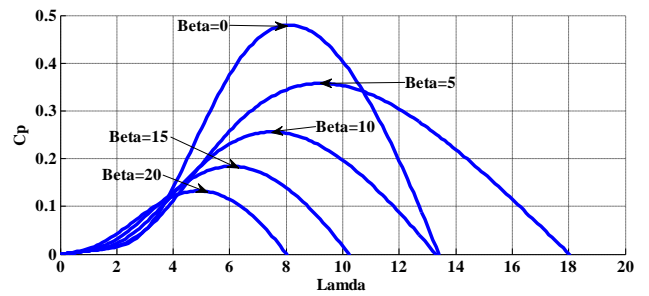

Fig. 2 Power coefficient $C_p(\lambda, \beta)$ versus λ for various values of pitch angle β.

So in the mode of MPPT which is between cut in wind speed and rated wind speed, If λ is maintained constantly at its optimal value corresponding to $C_{p,max}$, this ensures that the energy extracted is in its maximum operating point.
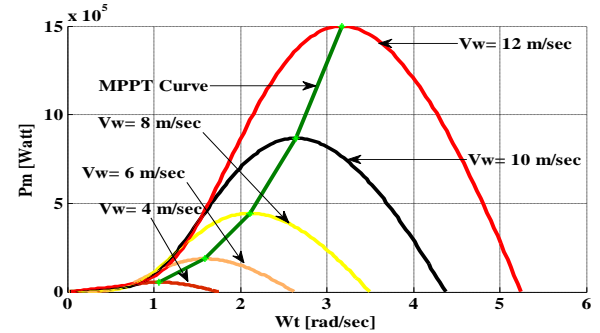

Fig. 3 Wind turbine mechanical power output and MPP versus turbine speed at different wind speed

Fig. 3 shows turbine mechanical power as a function of turbine speed by substituting (2), (3) and (4) in (1) at various wind speed and TSR λ. The power for a certain wind speed is maximum at a certain value of rotor speed called optimum turbine speed $w_{t,opt}$. This is the speed which corresponds to optimum tip speed ratio λ_{opt} and maximum power coefficient $C_{p,max}$. In order to have maximum possible power, the turbine should always operate at λ_{opt}. This is possible by controlling the rotational speed of the turbine so that it always rotates at

the optimum speed of rotation. The maximum power points curve is obtained as shown in Fig. 3. The objective of the MPPT operation mode is to maximize power extraction at low to medium wind speeds by following the maximum value of the wind power coefficient (C_{pmax} and λ_{opt}) as depicted in Fig. 3.

3. MPPT based on Tip Speed Ratio λ

For MPPT the optimal TSR λ_{opt} is determined at maximum power coefficient $C_{p,max}$ and zero pitch angle β by using (2). Equation (2) is optimized for different λ using optimization technique called GA in present work. The next section will describe the GA method.

4. Genetic algorithm optimization
A. Principles of genetic algorithm

The GA is a robust optimization technique based on natural selection [10-13]. The basic goal of GA is to optimize functions called fitness functions. GA-based approaches differ from conventional problem-solving methods in several ways. A simple GA starts with a population of solutions encoded in one of many ways. Binary encodings are quite common and are used in this paper. The GA determines each string's strength based on an objective function and performs one or more of three genetic operators on certain strings in the population. GA concepts could be adapted into the form that is suitable for computer implementation. These properties make GA robust, powerful, and data-independent. The following steps will explain the GA method.

1) The Initialization generates an initial random population consisting of individuals whose characteristics are coded by the string of zeros and ones (Encoding the variables into binary strings).
2) A fitness function based on a suitable performance criterion; calculate a fitness value for each string within the population (Evaluation).
3) The Reproduction based on a probability basis; choose pairs of individuals to bread offspring strings, where individuals with a higher fitness value will be selected than those with a lower fitness value (Best fitness).
4) The Crossover divides the binary coding of each parent into two or more segments and then combines to give a new offspring string that has inherited part of its coding from each parent (The crossover used here is one cut point method).
5) The Mutation inverse bits in coding of the offspring with a low probability.
6) If search goal is achieved, or an allowable generation is attained, stop. Otherwise return to step (2).

B. Genetic algorithm controller for MPPT mode

The GA controller is used in the region between the cut in speed and the rated wind speed to find the maximum power at different wind speeds. To find and track the MPP, you should get the optimal value of λ at maximum power coefficient and this is done by genetic algorithm to solve (2) at different values of λ. Noting that the pitch angle in this region is zero. The object function used here is one variable equation then it is very important to define constrains and the other parameters of GA as the following:

$$0 \le \lambda \le 13$$

Where $\lambda_{min} = 0$ and $\lambda_{max} = 13$

The parameters used for GA are given in Table 1.

Table 1
Parameters of GA

Genetic Algorithm Property	Value
Chromosome Length	16
Population Size	200
No. of Iterations (Generations)	150

The object function used here is given as in (5):

$$Function = C_p(\lambda) = 0.5176\left(\frac{116}{\lambda_i} - 5\right)e^{-\frac{21}{\lambda_i}} + 0.0068\lambda \quad (5)$$

Where $\frac{1}{\lambda_i} = \frac{1}{\lambda} - 0.035$ at $\beta = 0$. Then, the above equation is entered in the GA under mentioned conditions and the result value obtained after number of generations (Iterations) of power coefficient using GA is $C_{p,max} = 0.48$ as shown in Fig. 4. The TSR λ corresponding to $C_{p,max}$ is $\lambda_{opt} = 8.1$ is shown in Fig. 5.
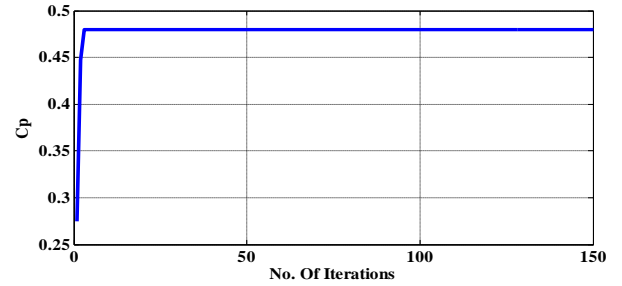

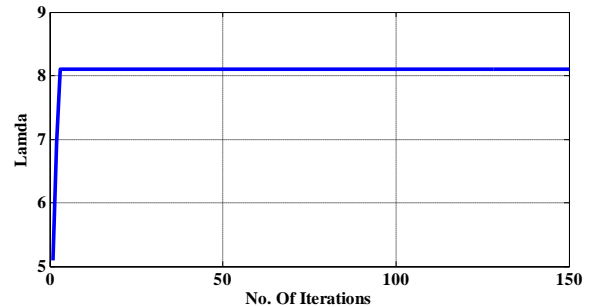Fig. 4 Maximum power coefficient versus number of iterations.

Fig. 5 Optimal value of λ versus number of iterations.

So, it is necessary to get the value of w_t which is corresponding to λ_{opt} at different wind speed at specified w_t corresponding to the maximum power that can be obtained using (1) as shown in Fig. 3.

5. MPPT using MATLAB/SIMULINK

The above equations used to track the maximum power point based on proposed GA are simulated using Matlab/Simulink as shown in Fig. 6.

Fig. 6 Block diagram of tracking curve in Matlab/Simulink.

The wind turbine parameters used here is shown in Table 2.

Table 2
Parameters of Wind Turbine

Parameter	Symbol	Value and Units
Air density	ρ	1.225 Kg/m^3
Rotor radius	R	30.6567 m
Number of blades	N_{blades}	3
Rated wind speed	$V_{Rated-wind}$	12 m/sec
Cut-in/cut-out wind speed	V_{cut-in} /$V_{cut-out}$	4/24 m/sec
Max C_p (MPPT)	C_{pmax}	0.48
Optimal λ (MPPT)	λ_{opt}	8.1
Gear ratio	R_{GB}	57.7996

6. Design of RSC controller for proposed MPPT under effect of changing wind speed

The proposed genetic MPPT technique is applied to DFIG through RSC. The DFIG model for WECS and design of RSC controller are described in the following sections.

A. DFIG model for WECS

The DFIG-based WECS is shown in Fig. 7. The dynamics of the DFIG is represented by a fourth-order state space model using the synchronously rotating reference frame (dq-frame) as given in (6)-(9) [14]. Where V_{qs}, V_{ds}, V_{qr} and V_{dr} are the q and d-axis stator and rotor voltages, respectively. I_{qs}, I_{ds}, I_{qr} and I_{dr} are the q and d-axis stator and rotor currents, respectively. λ_{qs}, λ_{ds}, λ_{qr} and λ_{dr} are the q and d-axis stator and rotor fluxes, respectively.

Fig. 7 DFIG based WECS.

$$V_{qs} = R_s I_{qs} + \omega_e \lambda_{ds} + \frac{d}{dt}\lambda_{qs} \qquad (6)$$

$$V_{ds} = R_s I_{ds} - \omega_e \lambda_{qs} + \frac{d}{dt}\lambda_{ds} \qquad (7)$$

$$V_{qr} = R_r I_{qr} + (\omega_e - \omega_r)\lambda_{dr} + \frac{d}{dt}\lambda_{qr} \qquad (8)$$

$$V_{dr} = R_r I_{dr} - (\omega_e - \omega_r)\lambda_{qr} + \frac{d}{dt}\lambda_{dr} \qquad (9)$$

ω_e is the angular velocity of the synchronously rotating reference frame. ω_r is the rotor electrical angular speed. R_s and R_r are the stator and rotor resistances, respectively.

The flux linkage equations are given as in (10)-(13):

$$\lambda_{qs} = L_s I_{qs} + L_m I_{qr} \qquad (10)$$
$$\lambda_{ds} = L_s I_{ds} + L_m I_{dr} \qquad (11)$$
$$\lambda_{qr} = L_r I_{qr} + L_m I_{qs} \qquad (12)$$
$$\lambda_{dr} = L_r I_{dr} + L_m I_{ds} \qquad (13)$$

Where L_s, L_r and L_m are the stator, rotor, and mutual inductances, respectively, with $L_s = L_{ls} + L_m$ and $L_r = L_{lr} + L_m$; L_{ls} and L_{lr} are the stator and rotor self inductance, respectively.

All the equations above are induction motor equations. When the induction motor operates as a generator, current direction will be opposite. The active and reactive power outputs from stator and rotor side are given as in (14)-(17):

$$P_s = \frac{3}{2}\left(V_{qs}I_{qs} + V_{ds}I_{ds}\right) \qquad (14)$$

$$Q_s = \frac{3}{2}\left(V_{qs}I_{ds} - V_{ds}I_{qs}\right) \qquad (15)$$

$$P_r = \frac{3}{2}\left(V_{qr}I_{qr} + V_{dr}I_{dr}\right) \qquad (16)$$

$$Q_r = \frac{3}{2}\left(V_{qr}I_{dr} - V_{dr}I_{qr}\right) \qquad (17)$$

The total active and reactive power generated by DFIG are given as in (18)-(19):

$$P_{total} = P_s + P_r \qquad (18)$$
$$Q_{total} = Q_s + Q_r \qquad (19)$$

If total P_{total} and/or total Q_{total} is negative, DFIG is supplying power to the power grid, else it is drawing power from the grid. The electromagnetic torque T_e generated by the machine which can be written in terms of flux linkages and currents is given as in (20):

$$T_e = \frac{3*P}{2}\left(\lambda_{ds}I_{qs} - \lambda_{qs}I_{ds}\right) \qquad (20)$$

Where P is the number of the pole pairs.

B. Design of RSC controller for proposed genetic MPPT

In DFIG wind energy systems, the stator of the generator is directly connected to the grid, and its voltage and frequency can be considered constant under the normal operating conditions. It is therefore, convenient to use stator voltage oriented control (SVOC) for the DFIG [15]. The stator voltage oriented control is achieved by aligning the d-axis of the synchronous reference frame with the stator voltage vector V_s. The resultant d- and q-axis stator voltages are: $V_{qs} = 0$ and $V_{ds} = V_s$. This DFIG control scheme is a rotor side control scheme where the active power is controlled by the direct current axis loop and the stator reactive power is controlled by the quadrature current axis loop. In the active power control loop the rotor electrical angular speed is compared with the reference rotor electrical angular speed obtained by MPPT. Then, the error is fed to a conventional PI (Speed Regulator) controller to generate the reference direct axis current. Where the proportional gain and the integral gain of the speed regulator are $K_{P,wr}$ and $K_{I,wr}$, respectively. Similarly, the stator side reactive power is calculated and is compared with the reference stator reactive power ($Q_{s,ref} = 0$). Then, the error is fed to another PI (Var Regulator) controller to generate the reference quadrature axis current. Where the proportional gain and the integral gain of the var regulator are $K_{P,Qs}$ and $K_{I,Qs}$, respectively. Then, both of the direct and quadrature axis reference currents are converted from d-q axis reference frame to a-b-c frame. Then, the three phase reference currents are compared with three phase rotor actual currents. Then, the error is the input to hysteresis current controller. Finally, the output of this controller is the switch control signals to the firing gate of RSC. The hysteresis controller output gives the switching pulses for the rotor side bidirectional converter control as shown in Fig. 8. The whole control scheme is simulated using Matlab/Simulink as shown in Fig. 9. The stator voltage vector angle θ_s is measured as shown in Fig. 10 and the rotor position angle θ_r is measured by an encoder mounted on the shaft of the generator. The slip angle θ_{sl} for the reference frame transformation can be obtained as the following ($\theta_{sl} = \theta_s - \theta_r$) as shown in Fig. 10.
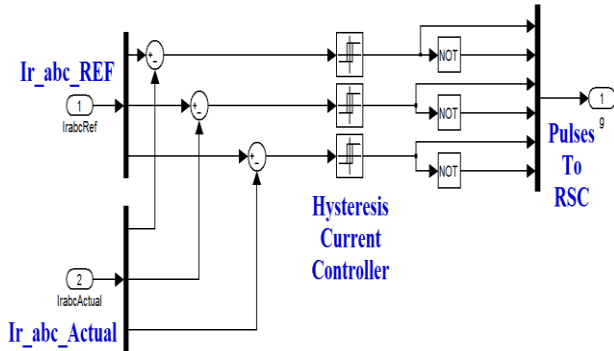
Fig. 8 Hysteresis current controller.
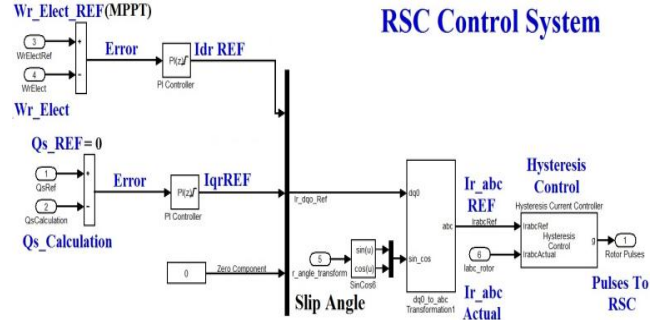
Fig. 9 Block diagram of RSC.
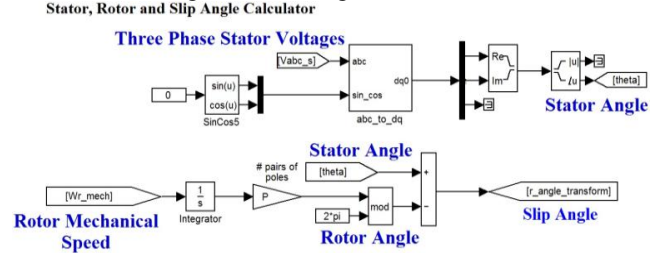
Fig. 10 Block diagram of stator, rotor and slip angle calculator.

C. Simulation results of RSC controller for step change in wind speed

Under varying wind speed the above described control system of RSC will prove its ability to get the required optimum rotor speed of generator corresponding to maximum output power. The next figures will show the effect of changing wind speed on MPPT. The wind speed varies as shown in Fig. 11. When the wind speed is less than rated speed ($V_w = 12\ m/sec$), the wind turbine is operating in MPPT mode so the steady state value of C_P is 0.48 (Maximum value) and λ is 8.1 (Optimum value) at $\beta = 0$. In this section, the system is controlled to track its maximum power operating point. Fig. 12 and 13 show the time response of C_p and λ due to wind speed variation, respectively. The rotor speed of generator is controlled according to MPPT strategy. When the wind speed varies, the rotor speed, the mechanical power, stator power and rotor power of generator response also varies as shown in Fig. 14 ,15 ,16 and 17, respectively. Also, the total active power output response of DFIG is shown in Fig. 18 but the stator reactive power response is always regulated to zero as depicted in Fig. 19. Achievement of unity power factor operation for RSC is illustrated in Fig. 20. It is clear from the figures the ability of RSC for achieving unity power factor at stator side and MPPT under different wind speeds.
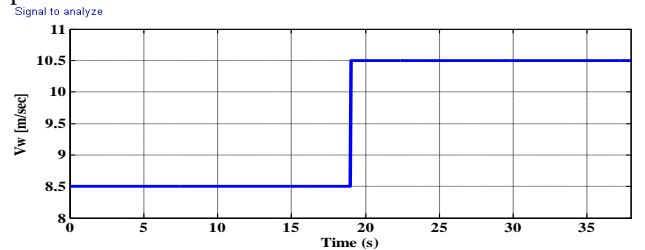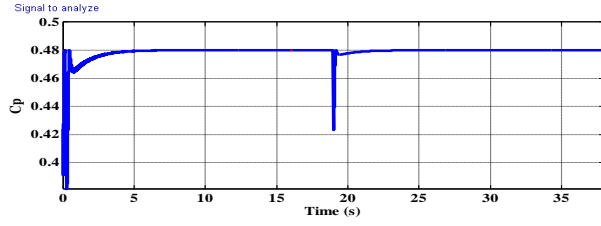

Fig. 11 Step change in wind speed.

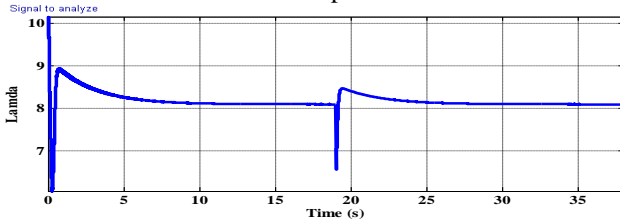Fig. 12 Power coefficient C_p response during the variation of wind speed.

Fig. 13 Tip speed ratio λ response during the variation of wind speed.
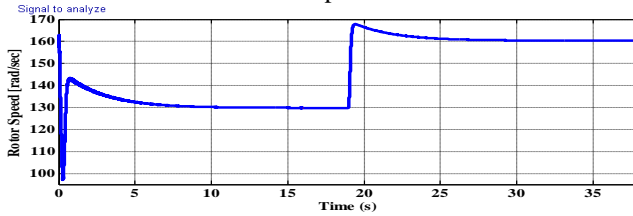

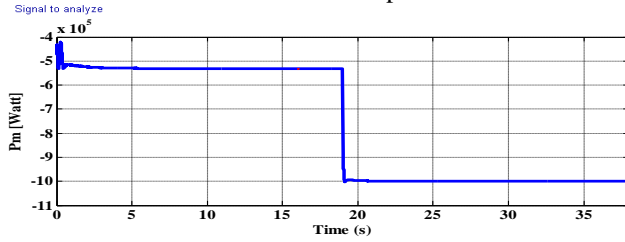Fig. 14 Rotor speed of generator response during the variation of wind speed.

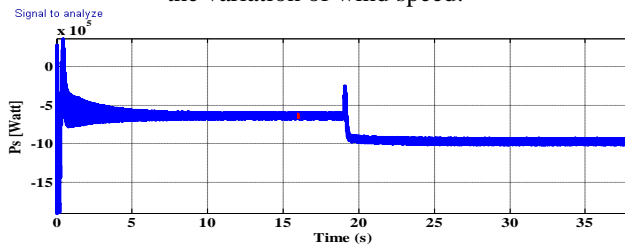Fig. 15 Mechanical power of generator response during the variation of wind speed.

Fig. 16 Stator active power response during the variation of wind speed.
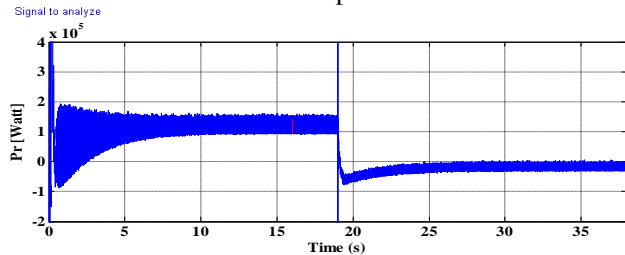

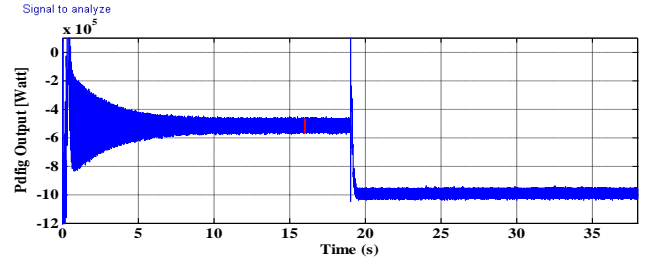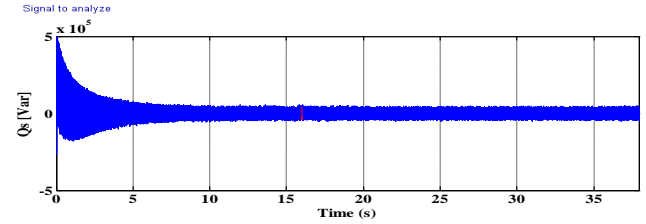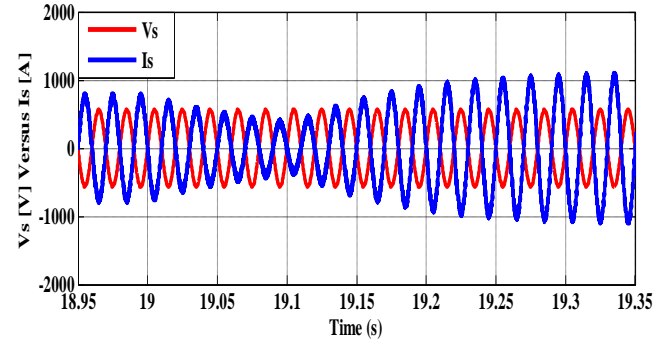Fig. 17 Rotor active power response during the variation of wind speed.

Fig. 18 Total active output power response generated by DFIG during the variation of wind speed.

Fig. 19 Stator side reactive power response during the variation of wind speed.

Fig. 20 Unity power factor by RSC for Phase A.

7. Design of GSC based SAPF for power quality improvement

The GSC has two functions, the first function is to maintain the DC-bus voltage constant at the required level for RSC, while the GSC currents should be sinusoidal and in phase with their counterparts voltages, for which the control system of DFIG maintains unity power factor condition and the second function is acting as SAPF to obtain unity power factor at power grid side due to presence of inductive load and get unity power factor and cancel current harmonic due to presence of nonlinear load at PCC connected in parallel with inductive load as shown in Fig 21. The proposed control algorithm of GSC adopts the SVO technique to regulate DC-link voltage and achieve a unity power factor at GSC side. This strategy leads to get and control the following active and reactive component of GSC fed to grid. This DFIG control scheme allows controlling the DC-bus voltage which is controlled by the direct current axis loop $I_{d-GSC-ref}$ and the quadrature current axis of GSC $I_{q-GSC-ref}$ which is kept at zero for unity power factor. First, the actual DC-bus voltage is compared with the reference DC-bus voltage.

Then, the error is fed to a conventional PI (DC Voltage Regulator) controller to generate the reference GSC direct axis current $I_{d-GSC-ref}$. Where the proportional gain and the integral gain of the DC voltage regulator are $K_{P,dc}$ and $K_{I,dc}$, respectively. Then, the reference compensated components of the load currents in d-q axis $I_{dc-load}$ and $I_{qc-load}$ which will be injected into the system are calculated as in below so the resulting reference d-q components of the load currents $I_{dc-load}$ and $I_{qc-load}$ must be subtracted from the direct and quadrature axis reference current of GSC $I_{d-GSC-ref}$ and $I_{q-GSC-ref}$ as shown in Fig. 22, respectively. After that, the result will be converted from d-q axis reference frame to a-b-c frame and these three phase currents will be compared with actual three phase currents of GSC through hysteresis controller. Finally, the output of hysteresis controller is the switch control signals to the firing gate of GSC as shown in Fig. 22. For the same condition of changing the wind speed mentioned before, it is clear from the next figures that the GSC has the ability to achieve DC voltage regulation of the DC link as shown in Fig. 23 and unity power factor at GSC side by keeping the quadrature axis current to zero as shown in Fig. 24.
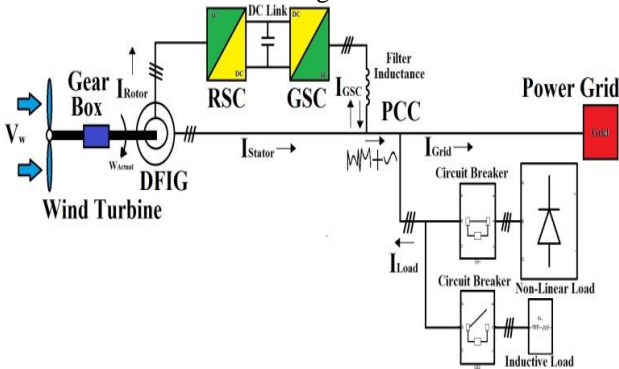
Fig. 21 Control principle of WECS with active filtering function.
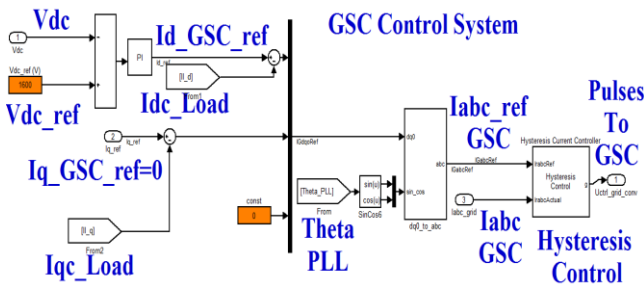
Fig. 22 Block diagram of GSC.
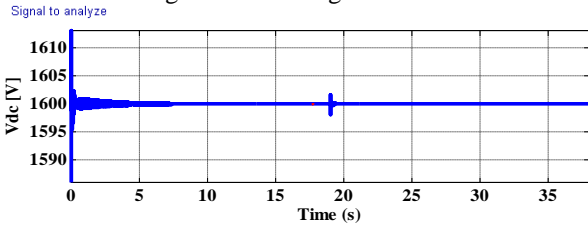
Fig. 23 The DC link voltage response during the variation of wind speed.
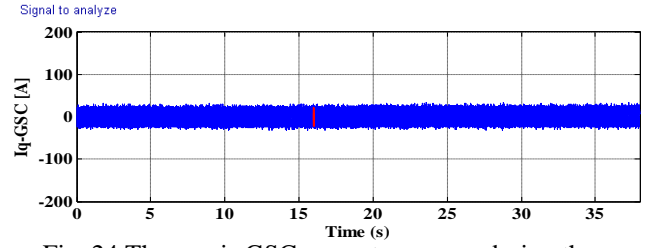
Fig. 24 The q-axis GSC current response during the variation of wind speed.

The present work tries to apply the GSC as shunt active filter for different loads such as nonlinear load and inductive load for power quality improvement. The SAPF will work with each load separately by using two circuit breaker as shown in Fig. 21. Frequency domain compensation, which is based on Fourier analysis, is not very used because it requires more real time processing power. There are various methods to identify the harmonic currents of a nonlinear load and phase shift of inductive load, the most classical methods are instantaneous power theory p-q, d-q synchronous detection method and Fryze current control [16]. It is known that the role of SAPF with three phase balanced power grid and balanced inductive load (Linear load) consuming reactive power which causes voltage drop and poor power factor is power factor correction and with non linear load is harmonic elimination and unity power factor. In this work, the synchronous reference frame d-q axis is used as shown in Fig. 25. Practically, in case of nonlinear load the direct axis compensation current $I_{dc-load}$ will contain on high frequency components that are extracted from the load current as shown in Fig. 25 and the quadrature axis compensation current $I_{qc-load}$ will contain on reactive fundamental component which is also extracted from the load current as shown in Fig. 25. The both of the two currents $I_{dc-load}$ and $I_{qc-load}$ will be used by GSC as shown in Fig. 22 to be injected into the system and will compensate the nonlinear load current components. Finally, after cancelling the high frequency component of the load current (Harmonics) and the reactive fundamental component of the load current the only remain component of the current at power grid side is the active fundamental component which will be in phase with power grid voltages and achieve unity power factor. Similarly, in case of inductive load the reactive power component of load current is extracted through quadrature axis compensation current $I_{qc-load}$ and in this case the direct axis compensation current $I_{dc-load}$ will be nearly zero. For being compensated by the GSC, the resulting d-q reference compensation currents ($I_{dc-load}$, $I_{qc-load}$) must be subtracted from the reference GSC direct and quadrature currents ($I_{d-GSC-ref}$, $I_{q-GSC-ref}$), respectively as shown in Fig. 22. Finally, After cancelling the phase shift produced by presence of reactive power the only remain component of the current at power grid side is the active fundamental

component which will be in phase with power grid voltages and achieve unity power factor.
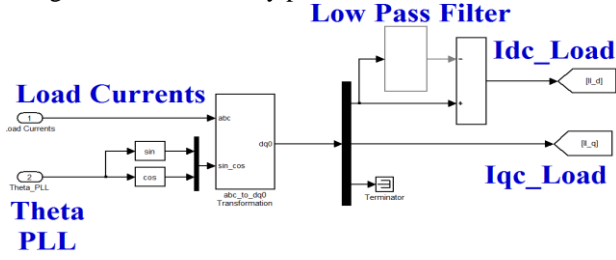
Fig. 25 Extraction of the load current components using d-q axis reference frame.

8. Design of PI controller for RSC and GSC

The output signal of a PI controller can be obtained by using (21):

$$U = K_P * e + K_I \int e * dt \qquad (21)$$

Where e is the error signal. K_P and K_I are the proportional gain and integral gain, respectively. There are some methods that can be used to determine the system parameters that can keep the whole system in the stable region. One of the methods is by using Butterworth polynomial to optimize the closed loop eigen value locations [17]. The Butterworth method locates the eigen values uniformly in the left-half s-plane on a circle with radius ω_o, with its center at the origin as shown in Fig. 26.
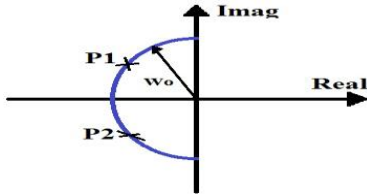
Fig. 26 Location of poles for second order Butterworth polynomial.

The Butterworth polynomial for a transfer function with a second order denominator is given as in (22):

$$p^2 + \sqrt{2} * \omega_o * p + \omega_o^2 = 0 \qquad (22)$$

Where $p = \frac{d}{dt}$. The PI parameters are determined by comparing the coefficients in (22) with the denominators of the corresponding transfer functions and then choosing appropriate ω_o. Where ω_o is the bandwidth of the controller, which depends upon the design value. The values of the parameters of each PI controller used in controlling of DFIG are shown in Table 3.

Table 3
Parameters of PI Controllers

	ω_o		628 rad/sec
RSC	Speed Regulator	$k_{P,Wr}$	17.7715
		$k_{I,Wr}$	7.8957
	Var Regulator	$k_{P,Qs}$	$5.7798*10^{-5}$
		$k_{I,Qs}$	0.0026
GSC	DC Voltage Regulator	$k_{P,dc}$	79.9719
		$k_{I,dc}$	3553.1

9. Digital simulation results for GSC

The overall model of DFIG control structure with nonlinear load which is three phase diode rectifier bridge inserted into its DC side RL load ($R_{l-dc} = 3.5750\Omega$ and $L_{l-dc} = 0.0501H$) and with balanced three phase inductive load ($R_l = 0.3\Omega$ and $L_l = 0.0045H$) connected in shunt with nonlinear load is simulated in Matlab/Simulink package. The two loads are connected to the power grid through two circuit breakers, the initial status of first circuit breaker at the AC side of nonlinear load is normally closed and its transition time is from 0 sec to 19 sec of simulation time and the initial status of the second circuit breaker at inductive load is normally open and its transition time is from 19 sec to 38 sec of simulation time. The simulation is carried out for step change in wind speed as the same waveform of wind speed mentioned before and the digital simulation results will be displayed for the two cases for phase A as the following:

1) Connecting SAPF alone at PCC with DFIG.
2) GSC based SAPF for enhancement of power quality.

A. Connecting SAPF alone at PCC with DFIG

The simulation is carried out for a 1.5 MW DFIG-based WECS with connecting SAPF at PCC as shown in Fig. 27. The DFIG parameters are shown in Table 4. Also, the SAPF parameters are shown in Table 5. The method used in designing SAPF is d-q axis synchronous reference frame.
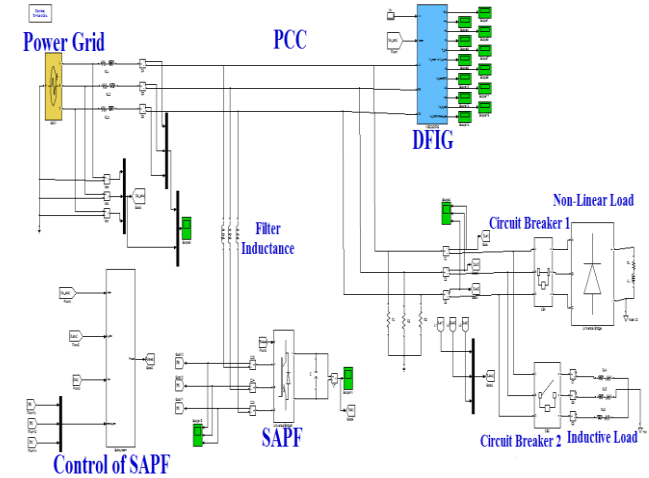

Fig. 27 Overall model of DFIG with connecting SAPF at PCC.

The considered load is connected at the PCC. So, the main goal is to eliminate the harmonic currents of the nonlinear load which has a Total Harmonic Distortion (THD) ratio of 27.84% during the period from 0 sec to 19 sec. The load current during the presence of nonlinear load will be square wave as shown in Fig. 28. As a result the current at power grid side will be distorted as shown in Fig. 29 which has THD ratio of 24.19% before connecting SAPF. When the SAPF is connected at PCC it will produce a current is called injection current as shown in Fig. 30. The injection current will cancel the high

frequency components and fundamental reactive component produced by nonlinear load and the only remain component is the fundamental active component which will be in phase with the voltage of power grid as shown in Fig. 31 and achieving unity power factor and free of harmonics. The THD ratio of the current at power grid side is 3.67%.
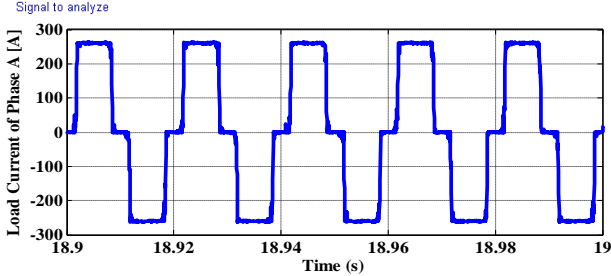

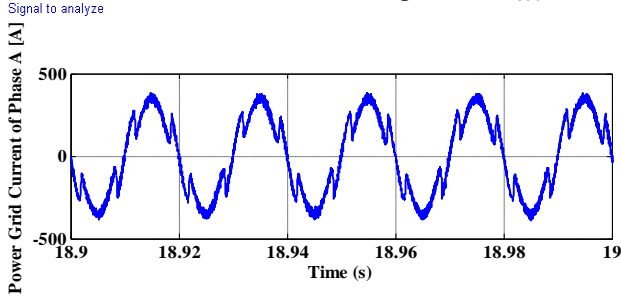
Fig. 28 Nonlinear load current of phase A $I_{load -A}$.

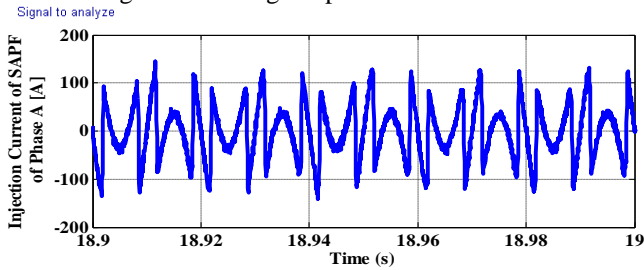Fig. 29 Power grid current of phase A $I_{Grid -A}$ before connecting SAPF during the presence of nonlinear load.

Fig. 30 Injection current of SAPF of phase A during the presence of nonlinear load.
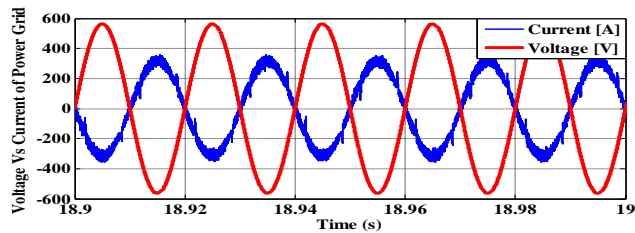
Fig. 31 Current versus voltage of power grid of phase A after connecting SAPF during the presence of nonlinear load.

Also, it is required to compensate the reactive power of the inductive load which has power factor equal to 0.2076 and produce reactive power equal to 0.634 MVar during the period from 19 sec to 38 sec. The load current during the presence of inductive load is shown in Fig. 32 which is

shifted from the grid voltage. Therefore, the current at power grid side will contain phase shift as shown in Fig. 33 before connecting SAPF. When the SAPF is connected at PCC it will generate an injection current as shown in Fig. 34. The injection current will cancel the phase shift produced by inductive load. So, the current at power grid side will be in phase with its voltage as shown in Fig. 35 and achieving unity power factor after cancelling the phase shift.
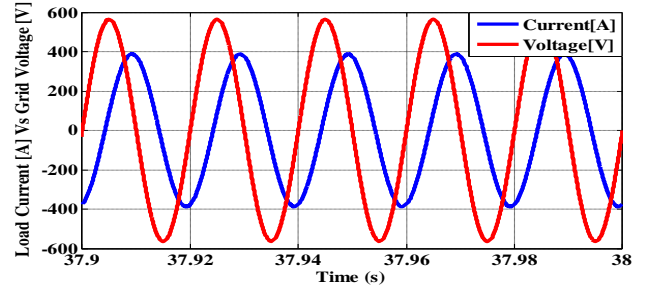

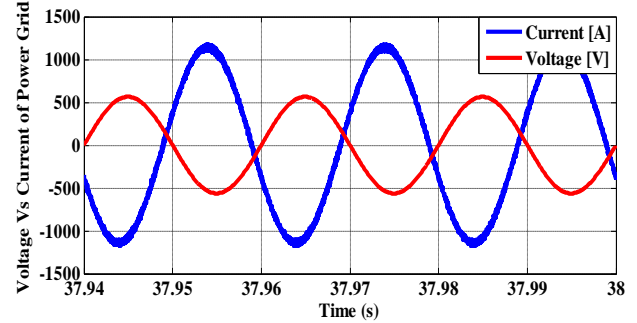Fig. 32 Inductive load current $I_{load -A}$ versus power grid voltage of phase A.

Fig. 33 Power grid current $I_{Grid -A}$ versus power grid voltage of phase A before connecting SAPF during the presence of inductive load.
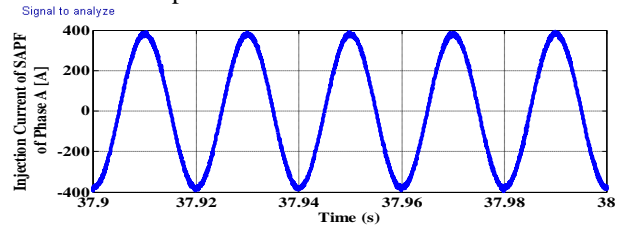

Fig. 34 Injection current of SAPF of phase A during the presence of inductive load.
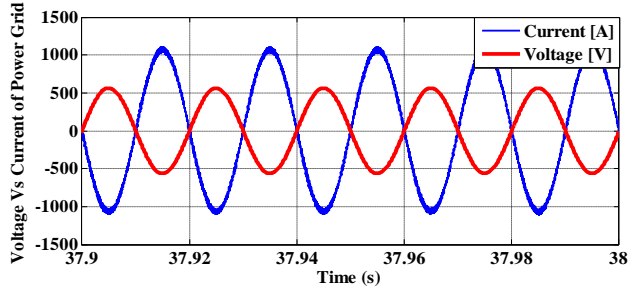

Fig. 35 Current versus voltage of power grid of phase A after connecting SAPF during the presence of inductive load.

Table 4
DFIG Parameters

Rated Mechanical Power	1.5 MW
Rated Stator Line-to-line Voltage	690 V (rms)
Rated Stator Frequency	50 Hz
Rated Rotor Speed	1750 rpm
Number of Pole Pairs	2
Rated Mechanical Torque	8.185 kN-m
Stator Winding Resistance, Rs	2.65 mΩ
Rotor Winding Resistance, Rr	2.63 mΩ
Stator Leakage Inductance, L_{ls}	0.1687 mH
Rotor Leakage Inductance, L_{lr}	0.1337 mH
Magnetizing Inductance, Lm	5.4749 mH
Shaft inertia	20 Kg. m^2
DC link voltage	1600 V
DC link capacitor	90 mF

Table 5
SAPF Parameters

Capacitor voltage V_{dc}	1600 V
Filter inductance	1 mH

B. GSC based SAPF for enhancement of power quality

The performance of DFIG WECS, in terms of active power filter, is studied for the same load as mentioned before. The overall simulation model of using GSC as SAPF is shown in Fig. 36.
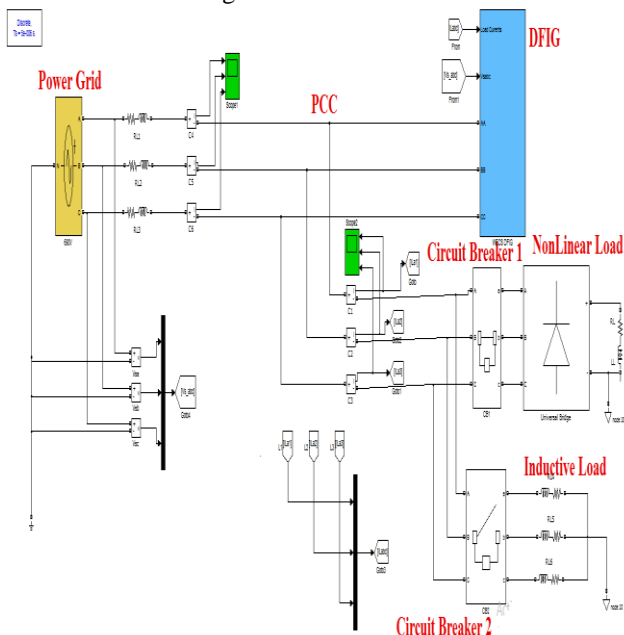

Fig. 36 Overall model using GSC of DFIG as SAPF in Matlab/Simulink.

The GSC will work as SAPF so it will be only with nonlinear load during the period from 0 sec to 19 sec so a current harmonic will pass into the system. So, before connection of GSC as SAPF the GSC current will be sinusoidal as shown in Fig. 37 and the power grid current

will be distorted and full of harmonics as shown in Fig. 38 which has a THD ratio of 24.19%. After connection of GSC as SAPF the GSC current will contain the required injection current to cancel harmonics and reactive fundamental component as shown in Fig. 39 therefore the power grid current will be sinusoidal and achieve unity power factor with its voltage and harmonic free as shown in Fig. 40. The THD ratio of the current at power grid side is 3.36%. During the period from 19 sec to 38 sec it will be only with the inductive load. So, before connection of GSC as SAPF the GSC current will be sinusoidal as shown in Fig. 41 and the power grid current will be not in phase with its voltage as shown in Fig. 42. After connection of GSC as SAPF the GSC current will include the required injection current to cancel the phase shift as shown in Fig. 43 therefore the power grid current will be sinusoidal and achieve unity power factor with its voltage as shown in Fig. 44.
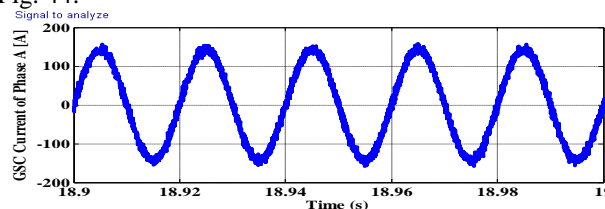

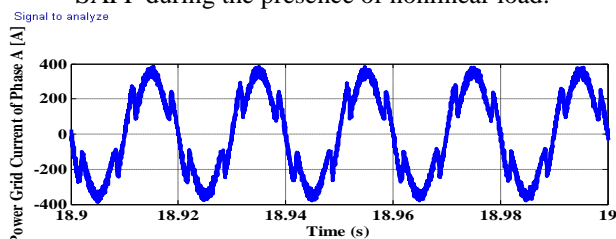Fig. 37 GSC current of phase A I_{GSC-A} without GSC as SAPF during the presence of nonlinear load.

Fig. 38 Power grid current of phase A I_{Grid-A} without GSC as SAPF during the presence of nonlinear load.
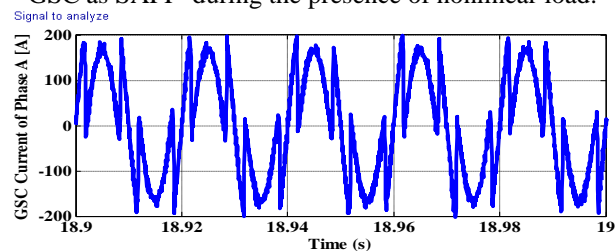

Fig. 39 GSC current of phase A I_{GSC-A} with GSC as SAPF during the presence of nonlinear load.
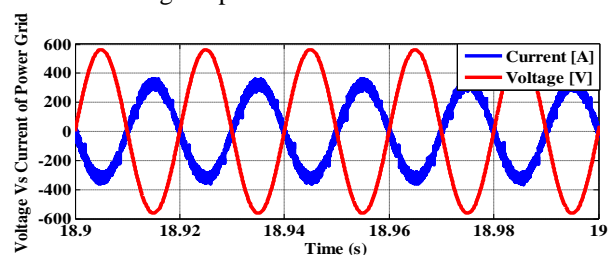

Fig. 40 Current versus voltage of power grid of phase A with GSC as SAPF during the presence of nonlinear load.
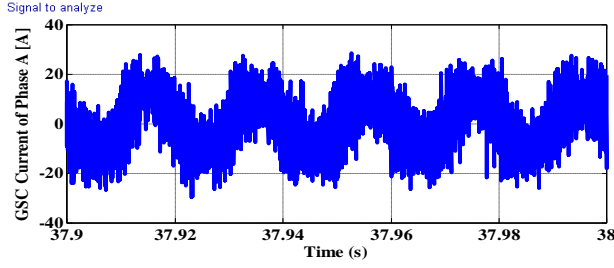
Fig. 41 GSC current of phase A I_{GSC-A} without GSC as SAPF during the presence of inductive load.
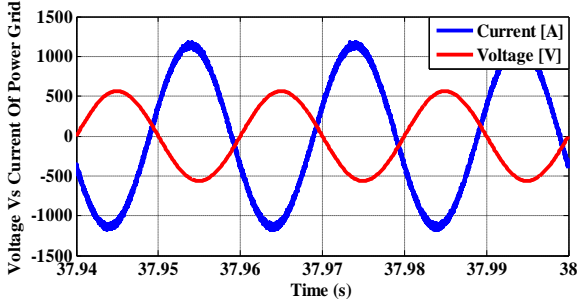

Fig. 42 Power grid current I_{Grid-A} versus power grid voltage of phase A without GSC as SAPF during the presence of inductive load.
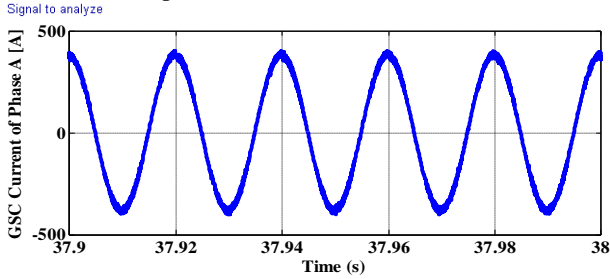

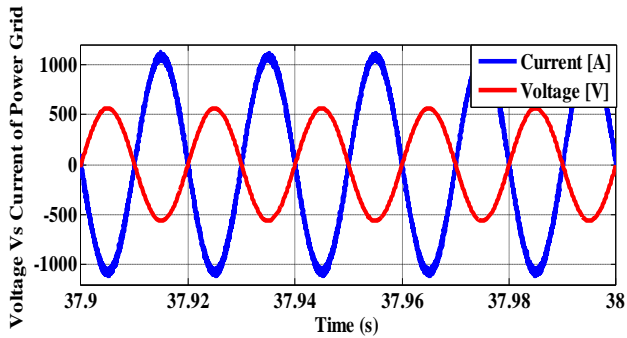Fig. 43 GSC current of phase A I_{GSC-A} with GSC as SAPF during the presence of inductive load.

Fig. 44 Current versus voltage of power grid of phase A with GSC as SAPF during the presence of inductive load.

It is clear from Table 6 that the THD ratio of power grid current in the case of connecting SAPF alone with DFIG is nearly equal the THD ratio in the case of GSC working as SAPF for the same current. The THD ratio for power grid current in both of the two cases is reduced compared to the case without connection of SAPF either alone or with GSC during the presence of nonlinear load at the period from 0 sec to 19 sec. Also, it is clear from Table

6 that reactive power at power grid side in the two cases either connection of SAPF either alone or with GSC is reduced by achieving unity power factor at this side compared to the case without connection of SAPF during the presence of inductive load at the period from 19 sec to 38 sec. it is obvious from this study that GSC as SAPF is better than connecting SAPF alone at PCC with DFIG from point of view the economic costing under mentioned conditions.

Table 6
Comparison between the values of THD and reactive power at power grid side before and after connection of two cases of SAPF

During presence of nonlinear load at period from 0 to 19 seconds			
Cases of connection	Before SAPF	After GSC as SAPF	After connecting SAPF alone
THD of power grid current	24.19%	3.36%	3.67%
During presence of inductive load at period from 19 to 38 seconds			
Reactive power at power grid side	0.634 MVar	0	0

10. Conclusion

In this paper, GA optimization method is used for the control of MPPT of the wind turbine by RSC. Also, GSC is used as SAPF to achieve power quality improvement. The GA is used in MPPT mode to get the optimal value of λ_{opt} and maximum power coefficient C_{pmax}. When the wind speed changes, this designed controller can track the maximum power when the wind speed is lower than the rated wind speed. Also, GSC is used as SAPF in addition to keeping the DC link voltage constant. The d-q synchronous reference frame axis is used in designing of SAPF to get the reference compensation components of currents to obtain unity power factor at power grid side, balanced three phase grid currents and harmonic free (reducing THD) in case of using nonlinear load and to compensate the phase shift for inductive load. Also, SAPF is connected alone at PCC with DFIG and results of this case are compared to the case of using GSC as SAPF and the total result of comparison shows that using GSC as SAPF is better than using SAPF alone for saving cost. The digital simulation results are carried out by using Matlab/Simulink package. The results show that the proposed controllers of DFIG give good performance and also show that GSC can work as SAPF and improve the power quality.

References

[1] H. Camblonga, I. Martinez de Alegriab, M. Rodriguezc, and G. Abadc, *"Experimental evaluation of wind turbines maximum power point tracking controllers, Energy Convers Manage"*. Vol.47, No 18-19, 2006, pp. 2846–2858.

[2] A. Gaillard, P. Poure, S. Saadate, *Reactive power compensation and active filtering capability of WECS with DFIG without any over-rating*, Wind Energy 13 (7) (2009) 603-614.

[3] A. Gaillard, P. Poure, S. Saadate, M. Machmoum, *Variable speed DFIG wind energy system for power generation and harmonic mitigation*, Renewable Energy 34 (6) (2009) 1545-1553.

[4] D.Chwa, Kyo-Bean, *"variable structure control of the active and reactive powers for a DFIG in wind turbines"*, IEEE Trans. on industrial applications. Vol-46, No-6, Nov-Dec-2010.

[5] Q. Wang and L. Chang, *"An intelligent maximum power extraction algorithm for inverter-based variable speed wind turbine systems,"* IEEE Trans. Power Electron., vol. 19, no. 5, pp. 1242-1249, Sept. 2004.

[6] E. Hau, *Wind Turbines: Fundamentals, Technologies, Application, Economics*, 2nd edition, Springer, 2005.

[7] Grisales, L. T., Lemus, C. G., and Sergio, S., *"Overall Description of Wind Power Systems"*, in ing. Cienc enero-junio., Vol. 10, pp. 99–126,2014.

[8] Thongam, J. S. and Ouhrouche, M. , *"MPPT Control Methods in Wind Energy Conversion Systems"*, in Intech open, Vol 15, pp. 339-360, June 2011.

[9] Zhe, C., et al., *"A Review of the State of the Art of Power Electronics for Wind Turbines,"* IEEE Transactions on Power Electronics, Vol. 24, pp. 1859-1875, 2009.

[10] Salami, M., Cain, G., *"The Quest for a New Computing Architecture Based on Genetic Algorithms"*, Proceedings of the Electrical Engineering Congress (EEC94) , Sydney, Australia, November 1994.

[11] Abdullah, M. A., Yatim, H. M. and Tan,C. W., *"Particle Swarm Optimization-Based Maximum Power Point Tracking Algorithm for WindEnergy Conversion System,* "in IEEE International Conference on Power and Energy (PECon), pp.978-1-4673-5019, December 2012.

[12] Chen, J. H. , Yau, H. T. , and Hung, W. , *"Design and Study on Sliding Mode Extremum Seeking Control of the Chaos Embedded Particle Swarm Optimization for Maximum Power Point Tracking in Wind Power Systems"*, in MDPI , Vol 7, pp. 1706-1720, March 2014.

[13] B. Vasumathi, S. Moorthi, " *Harmonic Estimation Using Modified ADALINE Algorithm with Time-Variant Widrow- Hoff (TVWH) Learning Rule*",

Computers & Informatics (ISCI), 2011 IEEE Symposium, 2011, pp.113-118.

[14] Krause, O. Wasynczuk, and S. D. Sudhoff, *Analysis of Electric Machinery and Drive Systems*, IEEE Press, Wiley-Interscience, John Wiley & Sons, Inc., New Jersey, 2002.

[15] S. Müller, M. Deicke, and R. W. De Doncker, *Doubly Fed Induction Generator Systems for Wind Turbines*, IEEE Industry Applications Magazine, Vol. 8, No. 3, 26-33, 2.

[16] H. Akagi, Y. Kanazawa, A. Nabae, *Instantaneous reactive power compensators comprising switching devices without storage components*, IEEE Trans. on Industrial Applications 20 (3) (1984) 625-630.

[17] Gan Dong, *"Sensorless and Efficiency Optimized Induction Machine Control with Associated Converter PWM Modulation Schemes,"* Ph.D. dissertation, Tennessee Technological University, Dec. 2005.